Journal of Organometallic Chemistry 886 (2019) 27–33

Contents lists available at ScienceDirect

Journal of Organometallic Chemistry

journal homepage: www.elsevier.com/locate/jorganchem

Communication

Chiral salen Mn (III) immobilized on ZnPS-PVPA through alkoxyl-triazole for superior performance catalyst in asymmetric epoxidation of unfunctionalized olefins

Jing Huang [a, b, *], Sirui Liu [a], Yan Ma [a], Jiali Cai [c, **]

[a] State Key Laboratory of Silkworm Genome Biology, College of Biotechnology, Southwest University, Chongqing, 400715, PR China
[b] Institute for Clean Energy & Advanced Materials, Southwest University, Chongqing, 400715, PR China
[c] College of Rongchang, Southwest University, Chongqing, 402460, PR China

ARTICLE INFO

Article history:
Received 2 December 2018
Received in revised form
28 January 2019
Accepted 5 February 2019
Available online 20 February 2019

Keywords:
Chiral Mn (III) salen
Heterogeneous catalyst
Asymmetric epoxidation
Click chemistry

ABSTRACT

Chiral salen Mn (III) catalysts anchored onto ZnPS-PVPA via click chemistry are prepared and applied in asymmetric epoxidations of unfunctionalized olefins. Superior catalytic performances (conv%, up to >99; ee%, up to >99) are achieved in the epoxidations of α-methylstyrene, styrene, indene and 1-octene. According to 6-cyano-2,2-dimethylchromene and 6-nitro-2,2-dimethylchromene, configuration of epoxides are reversed. And then the catalysts are selective in not only oxidative systems, but also substrates. Moreover, superior reusability (yield, 82%; ee, 86%) after recycling for nine times could also be obtained, which provide the potential application in industry.

1. Introduction

Epoxides are validated as being important synthons in the industrial application of several commodity compounds, as well as in the preparation of many intermediates, fine chemicals, and pharmaceuticals by virtue of their chemical versatility and reactivity [1–6]. Chiral salen Mn (III) complexes are more suitable for the epoxidation of olefins since they are attractive redox active systems and demonstrate a high catalytic activity and selectivity [7–11]. Although homogenous catalysts show high activity in the epoxidation of olefins, they often suffer from difficulty in recovery and reusability. To overcome these problems, considerable efforts have been devoted to immobilize these complexes on various supports such as zeolites, silica, organic polymers, clays, magnetic nanoparticles, ion-exchange resins and carbon nanotubes. Some chiral salen based Mn (III) complex heterogenized on silica matrix exhibit a relatively high enantioselectivity for epoxidation reaction and asymmetric borohydride reduction of ketones [12–20].

In recent decades, the development of sustainable oxidative procedures on the basis of solid catalysts is aiming at reducing the environmental impact of the epoxidation reaction. Extensive studies have revealed the high catalytic activity of various supported catalysts in a number of oxidation reactions. Resins, organic gels, and fibres are the polymeric organic materials which act as the conventional support for the immobilization of enzymes. But they create problem in disposal and show low reusability. On the other hand, inorganic supports such as porous silica gels are environmentally more acceptable, structurally more stable, and also chemically more resistant to organic solvents and microbial attacks over the organic supports. By the incorporation of organic ligand in the pores of the silica wall an organic-inorganic hybrid is formed which make the materials hydrothermally stable and hydrophobic and higher catalytic efficient during applications for organic process. These kinds of applications of these materials in reaction condition provides a synergistic means of an efficient approach of the reactants to metal sites, and suitable mesochannels to drive out the products for next recycles [21–25]. However, the catalytic activity of some of these heterogeneous catalysts decreases upon immobilization due to the reduction in accessibility of active sites [26–28]. Our group has also reported a series of superior Jacobsen's

* Corresponding author. State Key Laboratory of Silkworm Genome Biology, College of Biotechnology, Southwest University, Chongqing 400715, PR China.
** Corresponding author. College of Rongchang, Southwest University, Chongqing, 402460, PR China.
E-mail address: hj41012@163.com (J. Huang).

https://doi.org/10.1016/j.jorganchem.2019.02.008
0022-328X/

catalysts with hybrid materials as the supports in asymmetric epoxidation of unfunctionalized olefins, such as zirconium oligo-styrenylphosphonate-phosphate (ZSPP) and zirconium poly (styrene-phenylvinylphosphonate)-phosphate (ZPS-PVPA) and zinc poly (styrene-phenylvinyl- phosphonate)-phosphate (ZnPS-PVPA) as well as calcium poly (styrene-phenylvinylphos- phonate)-phosphate (CaPS- PVPA) [29–32].

In this study, we have been initiated to design chiral Jacobsen's

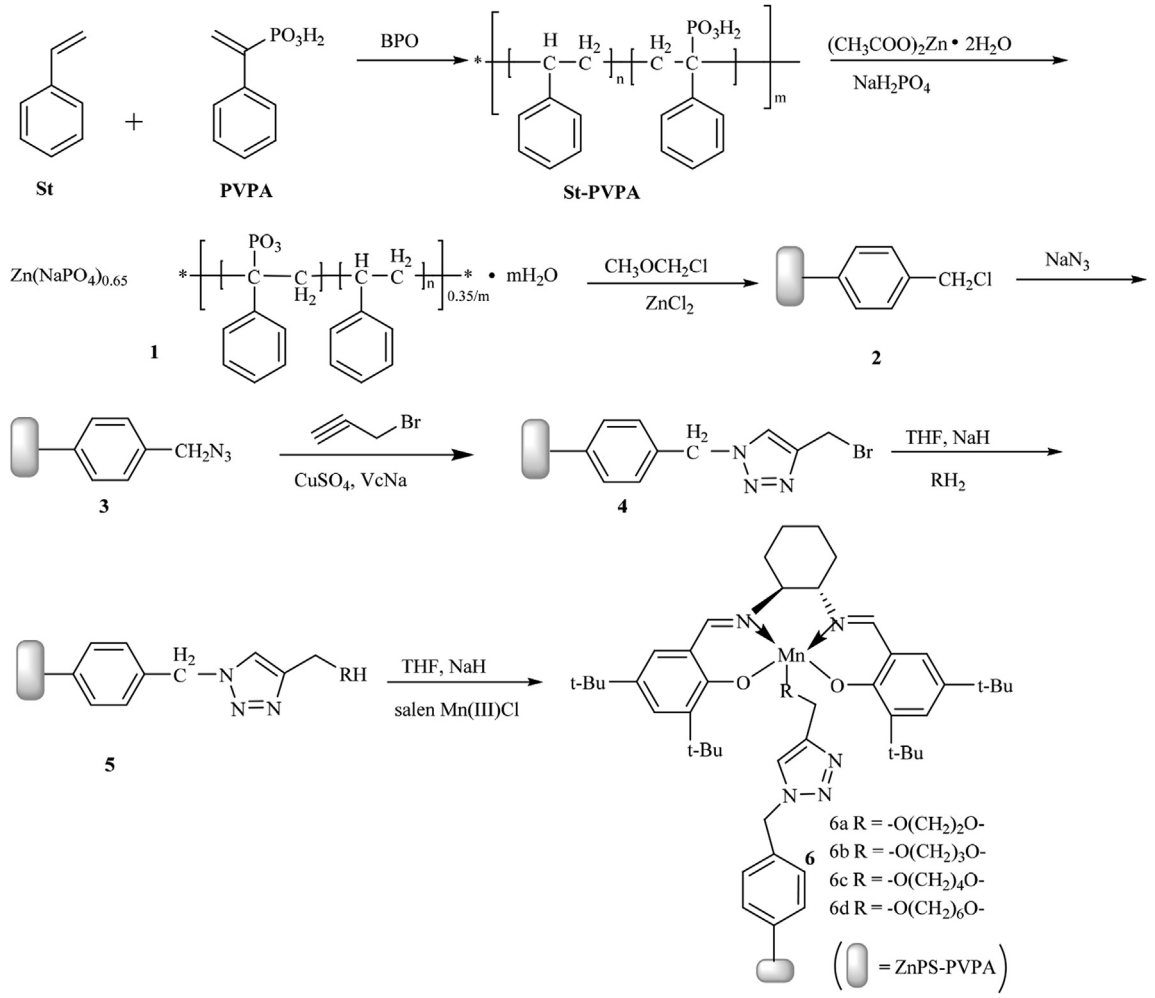

Scheme 1. Synthetic route of the heterogeneous catalysts.

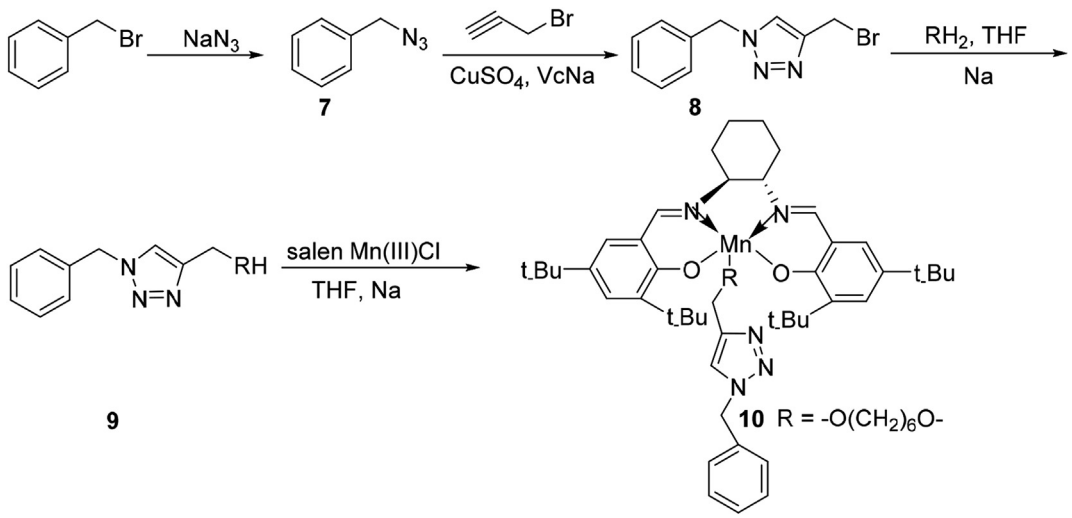

Scheme 2. The synthesis of homogeneous catalysts **10**.

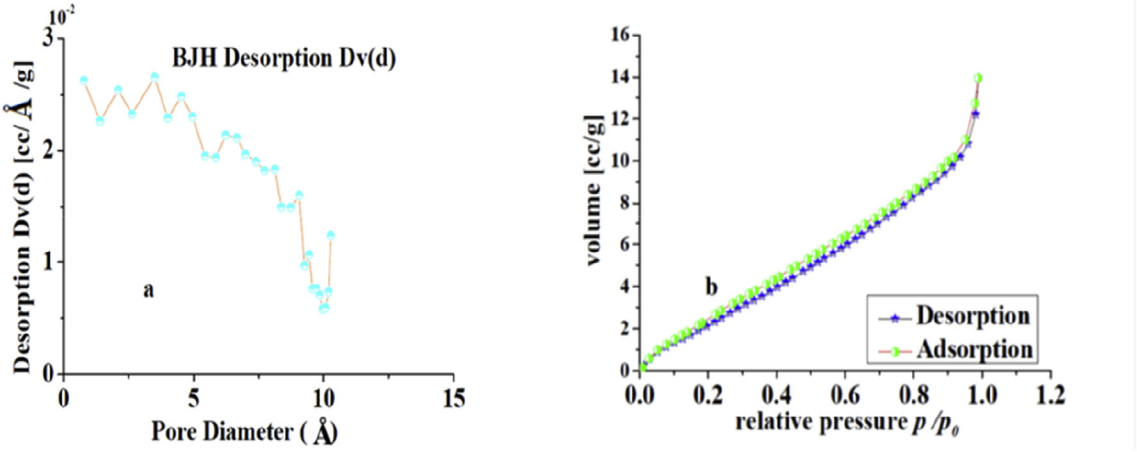

Fig. 1. The nitrogen adsorption-desorption isotherm and pore distribution of the catalyst **6d.**

catalysts immobilized on ZnPS-PVPA through alkoxyl-triazole (Scheme 1 and 2) for asymmetric epoxidation of unfunctionalized olefins. In addition, we also attempt to appraise the catalytic properties and to investigate the mechanisms as well as to explore the reusability.

As described in Fig. S1, both the catalysts 6a-d and Jacobsen's catalyst have displayed the same bands at 1620 cm^{-1} by virtue of the azomethene (C=N) stretching band. The bands at 523 cm^{-1} are due to the stretching vibration of Mn-O. The bands in the scope of 1345–1460 cm^{-1} for the catalysts are ascribed to the stretching vibration of C-H groups. The common prominent bands at 1145, 1089, and 986 cm^{-1} are attributed to R-PO_3^{2-} phosphonate stretching vibrations. The phosphonate and phosphate stretching vibrations are conductive to the adsorptions at 1200, 1145, and 1080 cm^{-1}. Apart from this, the bands at the hand of 1279 cm^{-1} refer to the vibration of triazole ring in the catalysts 6a-d. On account of this, the immobilization of Jacobsen's catalyst onto alkoxyl-modified ZnPS-PVPA has been confirmed successfully.

Based on the TG curves (Fig. S2), the initial weight loss is 2.5% below 200 °C, by virtue of surface-bound or intercalated water in this stage. And further decomposition of organic moieties contribute to 62.9% weight loss in the range of 200–550 °C. Finally, the small weight losses within the limits of 550–1000 °C are ascribed to exothermal transition. Therefore, the catalyst 6d still remains superior thermal stability near 180 °C.

In Fig. S3, the XRD patterns of ZnPS-PVPA indicate that a broad 001 peak (the lowest-angle diffraction peak in the pattern) at the vicinity of 24.8° is attributed to the parts of inorganic phosphate ($ZnNaPO_4$) in ZnPS-PVPA, and that other peaks at higher-order 00*n* peaks such as at 38.04° is ascribed to organic compositions in the catalysts. Although the intensities of all peaks for the catalyst 6d have weakened by virtue of the immobilization of Jacobsen's catalyst, the reflections also reveal that the mesoporous structure of ZnPS-PVPA still has been preserved. Simultaneously, the interlayer distance which could be calculated (*via* the Bragg equation, $n\lambda = 2d\sin\theta$) of the catalyst 6d (43.7 ± 0.1 Å) is nearly twice as much as that of ZnPS-PVPA (21 ± 1.3 Å). On account of this, it could be deduced that the augment of interlayer for the zinc layer is attributed to the introduction of chiral salen Mn (III) in ZnPS-PVPA, which is in contrast to the most of the results reported [29,30].

On account of the desorption isotherms (Fig. 1), the nitrogen adsorption-desorption isotherms belong to characteristic type V along with a sharp increase in N_2 adsorption at higher P/P_0 values (~0.9) and a distinct hysteresis loop (type H_3). Desorption isotherm is below adsorption isotherm, accompanying with an almost parallel adsorption and desorption. The pore diameters of the particles mainly vary from 2 nm to 12 nm, which is within the scope of mesoporous. And few particles are over 12 nm and less than 2 nm in diameter.

The corresponding textural parameters calculated by N_2 adsorption-desorption isotherms are presented in Table 1.

ZnPS-PVPA could offer sufficient space to contain the solvated chiral Mn (III) salen complex on account of the textural parameters in Table 1 (1 vs Jacobsen's: 3.5 vs 2.05–1.06 nm). Meanwhile, the physiochemical characterization data will be pulled out in two stages from ZnPS- PVPA to the catalyst: the first stage means that the textural parameters are on the increase through the chloromethylation and click chemistry as well as the alkoxylation, such as in BET surface area (1 vs 2 vs 4 vs 5, 4.9 vs 36.9 vs 38.7 vs 42.6 m^2/g), and in the pore volume (1 vs 2 vs 4 vs 5, 1.3 vs 18.82 vs 20.15 vs 23.57 × 10^{-2} cm^3/g) as well as in average pore diameter (1 vs 2 vs 4 vs 5, 3.5 vs 10.21 vs 12.78 vs 14.63 nm). This fact demonstrates that the effect on the textural parameters from the augment of the interlayer distance is stronger than the introduction of chloromethyl and triazolyl as well as alkoxy. On the contrary, the second stage refers to that the textural parameters begins to decrease by chance as a result of the immobilization of chiral salen Mn (III) on ZnPS-PVPA, for instance in BET surface area (5 vs 6d, 42.6 vs 14.18 m^2/g), and in the pore volume (5 vs 6d, 23.57 vs 2.16 × 10^{-2} cm^3/g) as well as in average pore diameter (5 vs 6d, 14.63 vs 6.09 nm), which is inconsistent with the results reported [29,30]. The introduction of sterically bulky salen Mn(III) in ZnPS-PVPA may aid in the occupation of some caves and holes as well as channels, which bring about the decrease of structure parameters.

The heterogeneous catalyst 6d reveals a Mn $2p_{3/2}$ core level peak at 642.6 eV (Fig. S4), which consists with the earlier literature data

Table 1
Physiochemical characterization data of 1–6.

Sample	Surface area (m^2/g)	Pore volum ($\times 10^{-2}$ cm^3/g)	Average pore diameter (nm)	Mn content (mmol/g)
1	4.9	1.3	3.5	–
2	36.9	18.82	10.21	–
4	38.7	20.15	12.78	–
5	42.6	23.57	14.63	–
6a	6a	10.26	1.85	5.72
6b	6b	11.57	1.92	5.86
6c	6c	12.31	2.03	5.91
6d	14.18	2.16	6.09	0.76

[33]. In comparison with the binding energy of 642.1 eV for neat chiral salen Mn(III) complex, the increase of 0.5 eV in chemical shift for the catalyst 6d is attributed to the diverse coordination microenvironment of Mn inside the configuration of the catalyst 6d.

SEM images indicate that the surface morphology transform from a smooth anomalous structure (ZnPS-PVPA, Fig. 2a)—a loose amorphous configuration (the catalyst 6d, Fig. 2b) by virtue of the immobilization of Jacobsen's catalyst. In view of the configuration of the catalyst 6d, there are many small caves and irregular channels, which would lead to the increase in surface area of the catalyst (6d vs ZnPS-PVPA, 28.02 vs 4.9 m^2/g) and further help the substrates to easily get closer with the catalytic sites.

TEM images of ZnPS-PVPA (Fig. 3a) reveals the spheroid structure with the sizes of the particle within the limits of 70–80 nm. On account of the catalyst 6d (Fig. 3b), the configuration is loose, and the channels, holes, cavums also exist. Based on this, the substrates are provided with more chance to approach the internal catalytic active sites and further symmetric epoxidation of unfunctionalized olefins could be carried out in sufficient space.

As for *m*-CPBA/NMO, ZnPS-PVPA and the alkoxyl-modified ZnPS-PVPA 5d are employed to catalyze asymmetric epoxidation of indene by way of investigating the chiral induction of the support and the linker (Table 2). Low olefin enantio excesses are achieved (ee%: ZnPS-PVPA vs 5d, 0 vs 26; entry 7 vs 8), which reveals that both ZnPS-PVPA and the alkoxyl-modified ZnPS-PVPA 5d are stereochemically inactive for the epoxidation of olefins. On account of the results reported, it could be deduced that the lower activity is ascribed to the absence of active catalysts on the exterior surface and a lack of any active solution species [10]. Simultaneously, ee values vary from 54% to 91% (Jacobsen's vs 10, entry 1 vs 10) owing to the alkoxylation and the introduction of 1,2,3-triazole, and further reach >99% (6d vs 10, entry 10 vs 5) by virtue of anchoring onto ZnPS-PVPA. Based on this, the synergistic effect originating from ZnPS-PVPA and the linkage alkoxyl-triazole as well as chiral salen Mn center contributes to the chirality of products.

According to NaClO/PPNO, the catalytic properties of the supported catalysts 6a-d are superior to Jacobsen's catalyst (conv%, 84 - >99 vs > 99; ee%, 73 - >99 vs 65; entry 12–15 vs entry 11). Moreover, the catalytic performance of homogeneous catalyst 10 have climbed to (conv%, 88; ee%, 93; entry 19) according to Jacobsen's catalyst (conv%, >99; ee%, 65; entry 11) due to the import of alkoxy and 1,2,3-triazole, and ultimately runs up to (conv%, >99; ee%, >99; entry 15) owing to the immobilization. This means that the coordination of ZnPS-PVPA, the linker including alkoxy and 1,2,3-triazole, and the chiral ligand acts on superior performance, which reveals that the appropriate conformation makes for the enantioselective oxygen transferring towards some substrates [33–35].

In view of $NaIO_4$/imidazole, no matter conversions or enantioselectivities according to the catalysts 6a-d all exceed 99%. Notably, ee values run up to 84% (the catalyst 10, entry 25) in contrast to 69% (Jacobsen's catalyst, entry 19) via alkoxy and 1,2,3-triazole, and at length attain >99% (6d, entry 23) as a result of anchoring onto ZnPS-PVPA. On account of this, it could be deduced that the catalytic properties are similarly ascribed to congenerous effect originating from ZnPS-PVPA and the linker as well as the chiral ligand.

Without the addition of NMO, ee value varies from 8% to >99%, conversion from 51% to >99% in the epoxidation of indene (entry 6 vs entry 5); ee from 20% to >99%, conversion from 62% to >99% in the epoxidation of α-methylstyrene (entry 32 vs 31); ee from 6% to

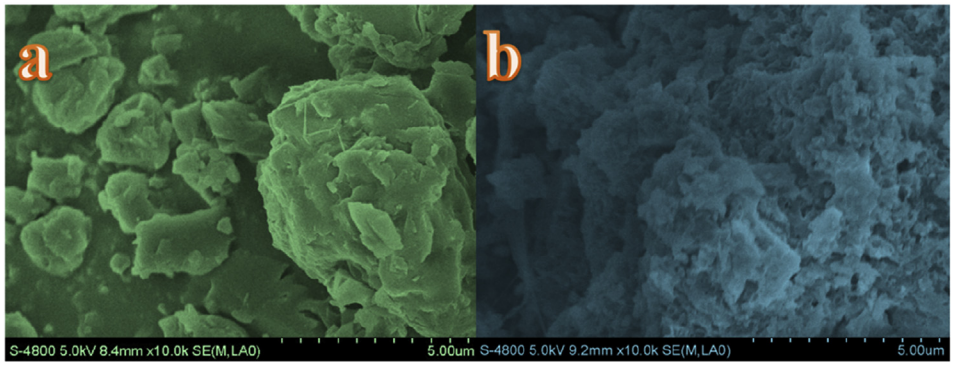

Fig. 2. SEM images of (a) ZnPS-PVPA and (b) the catalyst **6d**.

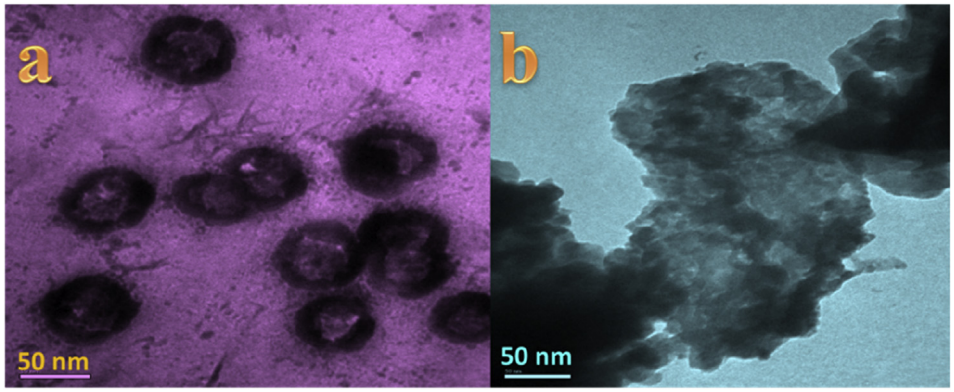

Fig. 3. TEM images of (a) ZnPS-PVPA and (b) the catalyst **6d**.

Table 2
Asymmetric epoxidation of alkenes catalyzed by **6a-d** and **10**.

Entry	Substrate[a]	Catalyst	Oxidant system	Time (h)	Conv. (%)	ee[e] (%)	TOF[f] $\times 10^{-4}(s^{-1})$
1	A	Jacobsen's	m-CPBA/NMO[b]	1	98	54	54.42
2	A	6a	m-CPBA	1	79	82	43.87
3	A	6b	m-CPBA	1	81	86	44.98
4	A	6c	m-CPBA	1	93	95	51.64
5	A	6d	m-CPBA	1	>99	>99	55.53
6	A	6d	m-CPBA/NMO	1	51	8	28.35
7	A	1	m-CPBA	1	>99	0	54.99
8	A	5d	m-CPBA	1	>99	26	54.99
9	A	10	m-CPBA/NMO	1	36	72	19.80
10	A	10	m-CPBA	1	97	91	53.34
11	B	Jacobsen's	NaClO/PPNO[c]	24	>99	65	2.31
12	B	6a	NaClO/PPNO	24	84	73	1.94
13	B	6b	NaClO/PPNO	24	86	85	1.99
14	B	6c	NaClO/PPNO	24	95	89	2.19
15	B	6d	NaClO/PPNO	24	>99	>99	2.31
16	B	6d	NaClO	24	63	75	1.46
17	B	10	NaClO/PPNO	24	88	93	2.03
18	B	10	NaClO	24	79	68	1.82
19	B	Jacobsen's	$NaIO_4$/imidazole[d]	5	>99	69	11.11
20	B	6a	$NaIO_4$/imidazole	5	>99	>99	11.11
21	B	6b	$NaIO_4$/imidazole	5	>99	>99	11.11
22	B	6c	$NaIO_4$/imidazole	5	>99	>99	11.11
23	B	6d	$NaIO_4$/imidazole	5	>99	>99	11.11
24	B	6d	$NaIO_4$	5	>99	>99	11.11
25	B	10	$NaIO_4$/imidazole	5	88	84	9.78
26	B	10	$NaIO_4$	5	82	80	9.11
27	B	Jacobsen's	m-CPBA/NMO	1	>99	54	54.99
28	B	6a	m-CPBA	1	84	72	46.19
29	B	6b	m-CPBA	1	88	81	48.39
30	B	6c	m-CPBA	1	93	86	51.14
31	B	6d	m-CPBA	1	>99	>99	54.99
32	B	6d	m-CPBA/NMO	1	62	20	34.09
33	C	Jacobsen's	m-CPBA/NMO	1	98	47	54.44
34	C	6a	m-CPBA	1	81	52	44.54
35	C	6b	m-CPBA	1	86	58	47.29
36	C	6c	m-CPBA	1	93	67	51.14
37	C	6d	m-CPBA	1	>99	74	54.99
38	C	6d	m-CPBA/NMO	1	>99	6	54.99
39	D	Jacobsen's	m-CPBA/NMO	1	90	40	50.00
40	D	6a	m-CPBA	1	82	61	45.09
41	D	6b	m-CPBA	1	85	69	46.74
42	D	6c	m-CPBA	1	92	73	50.59
43	D	6d	m-CPBA	1	>99	83	54.99
44	D	6d	m-CPBA/NMO	1	>99	8	54.99

[a] A = indene, B = α-methylstyrene, C = styrene, D = 1-octene.
[b] Reactions were carried out in CH_2Cl_2 (4 mL) with alkene (1 mmol), *n*-nonane (internal standard, 1 mmol), NMO (5 mmol), homogeneous (5% mmol) or heterogeneous salen Mn (III) catalysts (5% mmol) and *m*-CPBA (2 mmol) at 0 °C for 1 h. The conversions and the ee values were determined by GC with chiral capillary columns HP19091G-B 213, 30 m × 0.32 mm × 0.25 μm.
[c] Reactions were carried out in CH_2Cl_2 (2 mL) with alkene (0.5 mmol), *n*-nonane (internal standard, 89.3 μL, 0.5 mmol), PPNO (0.25 mmol) and NaClO (pH 11.3, 0.55 M, 1,25 mL) at 25 °C for 24 h.
[d] Reactions conditions: alkene (1 mmol), *n*-nonane (internal standard, 1 mmol), $NaIO_4$ (2 mmol), catalyst (0.03 mmol), CH_3CN/H_2O (10 mL/5 mL) at 25 °C for 5 h.
[e] (S)-form.
[f] Turnover frequency (TOF) is calculated by the expression of [product]/[catalyst] × time (s^{-1}).

74% in the epoxidation of styrene (entry 38 vs 37); ee from 8% to 83% in the epoxidation of 1-octene (entry 44 vs 43). The similar appearance also happens to homogeneous catalyst 10 (conv%, 36 vs 97; ee%, 72 vs 91; entry 9 vs 10) according to the epoxidation of indene. Namely, the addition of NMO to the reaction does not improve the chiral induction, but results in the decrease of the catalytic activity, which is adverse to the articles reported [29,30]. The framework of NMO is six-membered nitrogen and oxygen heterocycle with lone-pair electron, which is similar to that of 1,2,3-triazole involving five-membered nitrogen heterocycle with lone pair electrons. Evidently, NMO displays identical steric effect and electronic structure to 1,2,3-triazole. In the presence of NMO, the steric hindrance from 1,2,3-triazole impels the optimal geometric configuration of the reactive intermediates salen Mn(V)=O or their transition states altered, followed by the lower ee values.

No matter imidazole is added or not, ee values and conversions still reach >99% in the epoxidation of α-methylstyrene (entry 23 vs 24). As for the homogeneous catalyst, the performance increases a little in the presence of imidazole such as catalyst 10 (conv%, 88 vs 82; ee%, 84 vs 80; entry 25 vs 26). Imidazole is five membered nitrogen heterocycle with lone-pair electron, which is similar to the configuration of 1,2,3-triazole group. Distinctly, imidazole indicates slightly weak electronic effect and similar steric effect to 1,2,3-triazole group. Accordingly, the role of imidazole as the additive

to oxidation system $NaIO_4$/imidazole may be substituted by 1,2,3-triazole group in the heterogeneous catalyst and further superior performance could still be indicated with the addition of imidazole or not.

The addition of PPNO could still be conductive to the reinforcement of the catalytic properties (conv%, >99 vs 63; ee%, >99 vs 75, entry 15 vs 16), which agree with the articles reported [29,30,36]. The similar phenomenon has occurred to the homogeneous catalyst 10 (conv%, 88 vs 79; ee%, 93 vs 68; entry 17 vs 18). In this context, PPNO not only could heighten the stability of the catalyst through coordinating with salen Mn (III), but also could accelerate the speed of epoxidation in the way of transferring active ingredient HClO from aqueous phase to organic phase [37]. Apart from this, PPNO consists of benzene ring connected to pyridine ring, which owns nitrogen and oxygen atoms with lone-pair electron. On account of the whole effect from spatial orientation and the electron, PPNO is evidently stronger than 1,2,3-triazole group and further the role of PPNO could not be replaced by 1,2,3-triazole in reaction. In a word, superior performance could be obtained only when PPNO is added to the reaction system.

As for *m*-CPBA/NMO, ee values increase from 82% to 98%, conversions from 79% to >99% (entry 2–5) with the increase of chain length in asymmetric epoxidation of indene, which agree with the results reported by C. Li [36] and our group [30]. According to NaClO/PPNO, the catalytic performance also increase with the length of the linker in the epoxidation of α-methylstyrene (conv%, from 84 to >99; ee%, from 73 to >99; entry 12–15). This phenomenon could be interpreted that the heterogeneous salen Mn (III) catalysts may approach the active intermediates of salen Mn (V) or their transition states more easily owing to the elongation of chain length. While for $NaIO_4$/imidazole, the impacts originating from the chain length do not emerge. Both the conversions and enantioselectivities (entry 20–23) do not change with the increase of chain length and go beyond >99%, which demonstrates that superior oxidability of $NaIO_4$ hush up the effect of the chain length.

In Table 3, the catalyst 6a-d indicate higher catalytic performance than Jacobsen's catalyst in the epoxidation of 6-cyano-2,2-dimethylchromene (conv%, 68–98 vs 60; ee%, 63–87 vs 91; entry 2–5 vs 1) and 6-nitro-2,2-dimethyl-chromene (conv%, 71–97 vs 68; ee%, 69–85 vs 90; entry 7–10 vs 6). Moreover, the catalytic properties have also been boosted with the increase of chain length. For example, conversions increase from 68% to 98%, ee values from 63% to 87% in the epoxidation of 6-cyano-2,2-dimethylchromene (entry 2–5); conversions from 71% to 97%, ee values from 69% to 85% in the epoxidation of 6-nitro-2,2-dimethylchromene (entry 7–10).

On the other hand, the steric configuration of the epoxides (3S, 4S) catalyzed by 6a-d is obviously reversed in comparison with Jacobsen's catalyst (3R, 4R), which has been reported before [38]. As a matter of fact, the result is not only attributed to the linker, the support and the chiral ligand, but also related to the confinement effect deriving from the nanopores of the catalysts and the corresponding microenvironment. In this context, the interaction between the reactants and the products could hold back the reactants approaching the active site and further confine the rotation of the intermediates salen Mn(V)=O or transition states of the epoxidation [32,36], which finally affect the steric structure of the epoxides. Apart from this, the results in Table 2 reveal the same architecture of epoxides, which demonstrates that similar reaction mechanism process is carried out in asymmetric epoxidations of α-methylstyrene, indene, styrene and 1-octene. While for the epoxidation of 6-cyano-2,2-dimethylchromene and 6-nitro-2,2- dimethylchromene, the spatial framework of epoxides (3S, 4S) are turned according to Jacobsen's catalyst (3R, 4R), which confirms that the reagents assault or the groups leave in antipodal direction and then the reversal epoxides are formed. In brief, the survey also illustrates that the catalyst is selective about the substrates in asymmetric epoxidation of unfunctionalized olefins.

After nine consecutive times (Fig. 4), the catalytic performance reveals only a slightly decrease (conv%: from >99 to 82; ee%: from excess >99 to 86), which is still comparable to Jacobsen's catalyst (ee%, 54). The effective separation the chiral Mn (III) salen complexes by ZnPS-PVPA is conductive to the superior stability of the catalyst in case that they would dimerize to inactive μ-oxo-Mn (IV) species. Simultaneously, the decrease of properties could be mainly attributed to several factors, such as the decomposition of the catalysts under epoxidation conditions [32]; the desquamation of salen Mn (III) from ZnPS-PVPA as a result of stirring; the blockage of some pores and channels from byproduct in reaction. Apart from this, the Mn content of the catalyst 6d (0.45 mmol/g) slightly decreases after recycling for nine times, compared with the fresh catalyst (around 0.76 mmol/g).

In summary, we have explored a series of Jacobsen's catalyst anchored onto ZnPS-PVPA through alkoxy and 1,2,3-triazole. The superior catalytic performance in asymmetric epoxidation of unfunctionalized olefins (conv%, up to 99; ee%, up to 99) is due to

Table 3
Asymmetric epoxidation of 6-cyano-2,2-dimethylchromene and 6-nitro-2,2-dimethylchromene[a] catalyzed by **6a-d**.

Entry	Catalyst	Substrate[b]	Time (h)	Conv(%)	ee (%)[c]	TOF[d] × 10^{-4} (S^{-1})
1	Jacobsen's	D	6	60	91(3R, 4R)	5.56
2	6a	D	24	68	63(3S, 4S)	1.55
3	6b	D	24	76	72(3S, 4S)	1.75
4	6c	D	24	85	78(3S, 4S)	1.96
5	6d	D	24	98	87(3S, 4S)	2.26
6	Jacobsen's	E	6	68	90(3R, 4R)	6.30
7	6a	E	24	71	69(3S, 4S)	1.64
8	6b	E	24	78	72(3S, 4S)	1.80
9	6c	E	24	89	79(3S, 4S)	2.06
10	6d	E	24	97	85(3S, 4S)	2.24

[a] Reactions were carried out in CH_2Cl_2 (1 mL) with alkene (0.25 mmol), *n*-nonane (internal standard, 1 mmol), PPNO (0.05 mmol), homogeneous 5% mmol) or heterogeneous salen Mn(III) catalysts (5% mmol) and NaOCl (0.5 mmol).
[b] D = 6-cyano-2,2-dimethylchromene, E = 6-nitro-2,2-dimethylchromene
[c] Chiral HPLC OD column.
[d] Same as in Table 2.

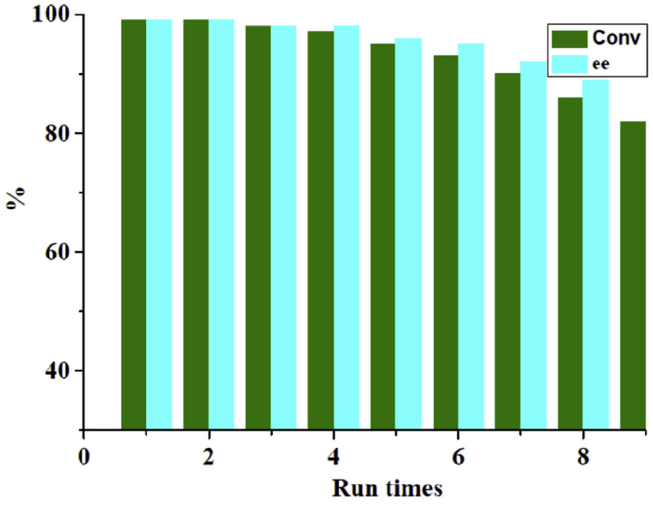

Fig. 4. The recycles of catalyst 6d in the epoxidation of α-methylstyrene.

the synergistic effect originating from ZnPS-PVPA and the linkage as well as chiral salen Mn (III) ligand. Moreover, the heterogeneous catalysts could still maintain comparable properties after recycling for nine times, which paves the way for the potential application in industry.

Acknowledgement

We gratefully acknowledge to the financial support from Faculty of Materials and Energy and Institute for Clean Energy & Advanced Materials, Southwest University and Chongqing Key Laboratory for Advanced Materials and Technologies of Clean Electrical Power Sources and the Fundamental Research Funds for the Central Universities (XDJK2013C120) and the Ministry of Education Chunhui Project (Z2016161) and the Recruitment Program of Southwest University, China (SWU117023).

Appendix A. Supplementary data

Supplementary data to this article can be found online at https://doi.org/10.1016/j.jorganchem.2019.02.008.

References

[1] M.A. Fardjahromi, M. Moghadam, S. Tangestaninejad, V. Mirkhani, I.M. Baltork, RSC Adv. 6 (2016) 20128.
[2] J.A. Birrell, E.N. Jacobsen, Org. Lett. 15 (2013) 2895.
[3] P.C.B. Page, C.J. Bartlett, Y. Chan, S.M. Allin, M.J. McKenzie, J. Lacour, G.A. Jones, Org. Biomol. Chem. 14 (2016) 4220.
[4] Y. Zhu, Q. Wang, R.G. Cornwall, Y. Shi, Chem. Rev. 114 (2014) 8199.
[5] R.M. Reich, M. Kaposi, A. Pöthig, F.E. Kühn, Catal. Sci. Technol. 6 (2016) 4970.
[6] S. Muratsugu, Z. Weng, M. Tada, ACS Catal. 3 (2013) 2020.
[7] A.M. Garcia, V. Moreno, S.X. Delgado, A.E. Ramírez, L.A. Vargas, M.Á. Vicente, A. Gil, L.A. Galeano, J. Mol. Catal. Chem. 416 (2016) 10.
[8] H.D. Zhang, Y. Zou, Y.M. Wang, Y. Shen, X.X. Zheng, Chem. Eur J. 20 (2014) 7830.
[9] F. Teixeira, R.A. Mosquera, A. Melo, C. Freire, M.N.D.S. Cordeiro, J. Phys. Chem. 118 (2014) 10788.
[10] P. McMorn, G.J. Hutchings, Chem. Soc. Rev. 33 (2004) 108.
[11] Y.C. Zhang, Q. Zhou, W.C. Ma, J.Q. Zhao, Catal. Commun. 45 (2014) 114.
[12] K. Gupta, A.K. Sutar, Coord. Chem. Rev. 252 (2008) 1420.
[13] R.I. Kureshy, N.H. Khan, S.H. R Abdi, I. Ahmad, S. Singh, R.V. Jasra, J. Catal. 221 (2004) 234.
[14] M. Moosavifar, S. Tangestaninejad, M. Moghadam, V. Mirkhani, I.M. Baltork, J. Mol. Catal. Chem. 377 (2013) 92.
[15] A. Mavrogiorgou, M. Papastergiou, Y. Deligiannakis, M. Louloudi, J. Mol. Catal. Chem. 393 (2014) 8.
[16] N.E. Thornburg, A.B. Thompson, J.M. Notestein, ACS Catal. 5 (2015) 5077.
[17] A. Corma, H. Garcia, Adv. Synth. Catal. 348 (2006) 1391.
[18] R.I. Kureshy, I. Ahmad, N.H. Khan, S.H. R Abdi, K. Pathak, R.V. Jasra, Tetrahedron: Asymmetry 16 (2005) 3562.
[19] I.D. Hierro, Y. Pérez, M. Fajardo, Microporous Mesoporous Mater. 263 (2018) 173.
[20] R.I. Kureshy, N.H. Khan, S.H. R Abdi, S. Singh, I. Ahmad, R.V. Jasra, A.P. Vyas, J. Catal. 224 (2004) 229.
[21] Y.J. Chen, R. Tan, Y.Y. Zhang, G.W. Zhao, W.G. Zheng, R.C. Luo, D.,H. Yin, Appl. Catal., A 491 (2015) 106.
[22] W.G. Zheng, R. Tan, S.F. Yin, Y.Y. Zhang, G.W. Zhao, Y.J. Chen, D.H. Yin, Catal. Sci. Technol. 5 (2015) 2092.
[23] K. Zhang, O.K. Farha, J.T. Hupp, S.T. Nguyen, ACS Catal. 5 (2015) 4859.
[24] D. Munz, D.Y. Wang, M.M. Moyer, M.S.W. Gardiner, P. Kunal, D. Watts, B.G. Trewyn, A.N. Vedernikov, T.B. Gunnoe, ACS Catal. 6 (2016) 4584.
[25] L. Paul, B. Banerjee, A. Bhaumik, M. Ali, Microporous Mesoporous Mater. 249 (2017) 78.
[26] M. Liu, Z.P. Zhao, K.C. Chen, W.F. Liu, Catal. Commun. 64 (2015) 70.
[27] F.Z. Zhang, X.F. Zhao, C.H. Feng, B. Li, T. Chen, W. Lu, X.D. Lei, S.L. Xu, ACS Catal. 1 (2011) 232.
[28] R.I. Kureshy, I. Ahmad, N.H. Khan, S.H.R. Abdi, K. Pathak, R.V. Jasra, J. Catal. 238 (2006) 134.
[29] W.S. Ren, X.K. Fu, H.B. Bao, R.F. Bai, P.P. Ding, B.L. Sui, Catal. Commun. 10 (2009) 788.
[30] B.W. Gong, X.K. Fu, J.X. Chen, Y.D. Li, X.C. Zou, X.B. Tu, P.P. Ding, L.P. Ma, J. Catal. 262 (2009) 9.
[31] J. Huang, X.K. Fu, G. Wang, Q. Miao, Dalton Trans. 41 (2012) 10661.
[32] J. Huang, X.K. Fu, Q. Miao, Appl. Catal., A 407 (2011) 163.
[33] A.R. Silva, J.L. Figueiredo, C. Freire, B. Castro, Microporous Mesoporous Mater. 68 (2004) 83.
[34] V.L.P. Fragola, F. Lupo, A. Pappalardo, G.T. Sfrazzetto, R.M. Toscano, F.P. Ballistreri, Gaetano A. Tomaselli, A. Gulino, J. Mater. Chem. 22 (2012) 20561.
[35] G.T. Sfrazzetto, S. Millesi, A. Pappalardo, R.M. Toscano, F.P. Ballistreri, G.A. Tomaselli, A. Gulino, Catal. Sci. Technol. 5 (2015) 673.
[36] H.D. Zhang, Y.M. Zhang, C. Li, J. Catal. 238 (2006) 369.
[37] D.L. Hughes, G.B. Smith, J. Liu, G.C. Dezeny, C.H. Senanayake, R.D. Larsen, T.R. Verhoeven, P.J. Reider, J. Org. Chem. 62 (1997) 2222.
[38] R. Raja, J.M. Thomas, M.D. Jones, B.F.G. Johnson, D.E.W. Vaughan, J. Am. Chem. Soc. 125 (2003) 14982.